Optimum parallel-face slanted surface-relief gratings

Jonathan S. Maikisch* and Thomas K. Gaylord

School of Electrical and Computer Engineering and Microelectronics Research Center, Georgia Institute of Technology, Atlanta, Georgia 30332-0250, USA

*Corresponding author: gtg194z@mail.gatech.edu

Received 27 November 2007; accepted 16 February 2007;
posted 12 March 2007 (Doc. ID 77344); published 31 May 2007

Using a combination of rigorous coupled-wave analysis and simulated annealing, parallel-face slanted surface-relief gratings (PFSSRGs) are optimized. For substrate-mode optical interconnects, profiles are presented for both polymer and silicon PFSSRGs for both TE and TM polarizations at normal incidence with grating periods designed to give a 45° output angle in the negative-first forward-diffracted order. The resulting diffraction efficiencies range from 70% to 99%, with a majority of the optimized profiles yielding over 90%. Optimized polymer profiles for TE and TM polarizations exhibit similar high diffraction efficiencies, but the TM profiles generally require greater groove depths. Silicon profiles optimized for TM polarization have greater diffraction efficiencies than those for TE polarization. Profiles that can feasibly be fabricated are identified, and sensitivities to groove depth, filling factor, slant angle, and incident angle are shown to be modest.

OCIS codes: 050.0050, 050.1950, 230.1950.

1. Introduction

Surface-relief gratings (SRGs) are of great interest in many applications, including disk pickup heads [1], optical interconnect couplers [2–7], quantum-well infrared photodetectors [8], chemical and biological sensors [9,10], silicon photonics [11], and other applications that require an efficient redirection of light. Parallel-face slanted surface-relief gratings (PFSSRGs) offer the possibility of large first-order diffraction efficiencies with grating feature sizes of the order of a wavelength. SRGs are typically fabricated via a masking technique such as optical interferometry in a photoresist combined with reactive-ion etching [2,12], nanoimprinting with a premade mold [13], or direct electron-beam lithography [14]. However, the fabrication technique chosen affects the range of slant angles and groove depths that can be realized. Referring to the PFSSRG in Fig. 1, it is clear that overhanging grooves may greatly complicate the fabrication process.

With the availability of new and improved fabrication techniques, the fabrication of some of the more challenging PFSSRG profiles can now be accomplished. For semiconductor and polymer profiles, slanted reactive-ion etching is able to etch profiles with moderate slants and depths. If the polymer in question is a photopolymer such as azobenzene, optical lithography [15] can also be used. A promising new technique for both polymers and semiconductors is energetic neutral atom beam lithography and epitaxy (ENABLE) [16]. By using an energetic beam of neutral oxygen atoms, a polymer that forms a volatile product with oxygen can be etched, and masking can be performed by another material that does not form a volatile product with oxygen. Profiles in semiconductor materials can be achieved by deposition and lift-off with a polymer template [17], and the use of ENABLE also allows for low-temperature deposition of nitride and oxide materials [18]. The smallest achievable feature size is limited primarily by the masking technique used, and the problem of etched feature degradation due to charge spreading is solved by the use of a neutral atomic beam.

Optimization for PFSSRGs is critical in order to make efficient use of the aforementioned fabrication methods. To optimize a PFSSRG profile for a given application, a systematic method is required that will not overlook possible optimized profiles while simultaneously not requiring excessive simulation time. It is also important that the optimization technique be

0003-6935/07/183674-08$15.00/0

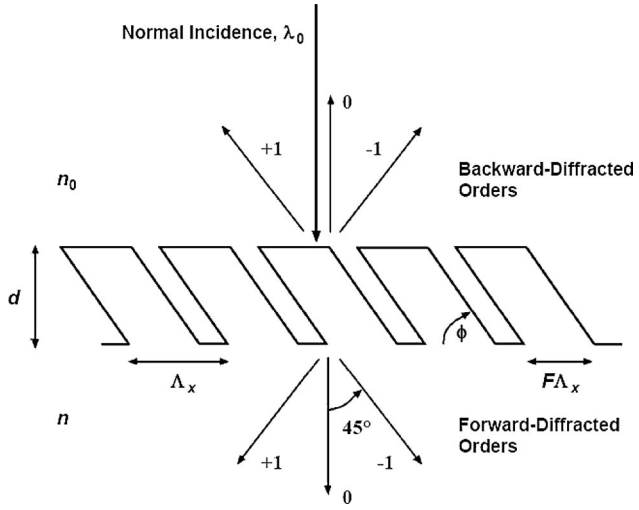

Fig. 1. Configuration of a PFSSRG illuminated by normally incident light. The PFSSRGs are characterized by the grating period Λ_x (which is determined by choosing an output angle of 45° for the negative-first diffracted order), the groove depth d, the slant angle ϕ, and the filling factor F. The substrate refractive index is n, and the input region index is n_0 (air in our case).

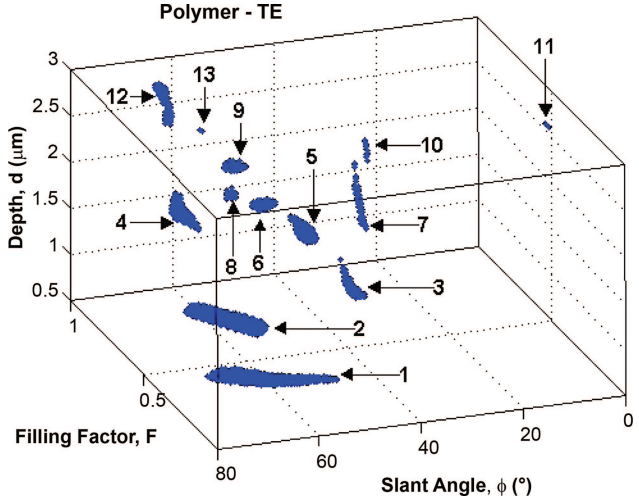

Fig. 2. (Color online) Mapped points for polymer PFSSRGs in TE operation with diffraction efficiencies greater than 94.73% in the negative-first order. There are 13 identified regions with local optima.

applicable for a broad range of uses, including those that are not concerned solely with highly efficient diffraction into one diffractive order. Rigorous coupled-wave analysis (RCWA) has been used extensively by Moharam and Gaylord [19,20] to optimize and characterize various grating cases but not including PFSSRGs. Also utilizing RCWA, Wu *et al*. [21,22] have incorporated the use of a simulated-annealing (SA) algorithm to reduce simulation time while investigating sawtooth and trapezoidal SRG cases. Wang, Jiang, and Nordin [23–25] have focused specifically on PFSSRGs using a microgenetic two-dimensional finite-difference time-domain (μGA-2D FDTD) approach. Their focus was on the strong coupling regime in which a fiber couples into a waveguide or vice versa. While very accurate, their method is hindered by long simulation times, which they have addressed with a streamlined design process [25] that requires some arbitrary fixing of parameters. While previous work on optimization of PFSSRGs has demonstrated an ability to locate optimum profiles within a simulation space, it is nevertheless desirable to characterize a simulation space by *all* of its potential optimum profiles if multiple optima exist. While doing this, it is also important to choose a means of simulation that will allow for the desired accuracy without requiring excessive simulation time.

In this paper, by using a combination of RCWA analysis and an SA algorithm, we demonstrate the efficient optimization of polymer and silicon PFSSRGs and the characterization of the simulation space with multiple optimum profiles.

2. Previous Surface-Relief Grating Optimization

Moharam and Gaylord [19,20] provided extensive work on the optimization of various SRG profiles (not including the PFSSRG case) with RCWA. Diffraction efficiencies of up to 99% in the first order with incidence at the first Bragg angle, TE propagation, and $\lambda = \Lambda_x$ ($n = 1.58$) were achieved. Wu *et al*. [21] have utilized an SA algorithm in conjunction with RCWA for anisotropically etched trapezoidal silicon profiles for TE and TM polarizations and normal incidence. The only fixed parameters in this work were the slant angle (54.736° fixed by anisotropic etching) and the grating period (fixed by the 45° diffraction angle). Efficiencies were limited to 67.1% for TM polarization and 37.3% for TE polarization. Furthermore, Wu *et al*. [22] applied the same method to the analysis of sawtooth gratings and trapezoidal gratings without fixed slant angle for both silicon and a representative polymer. The sawtooth case only required variation in one parameter: the groove depth. The trapezoidal

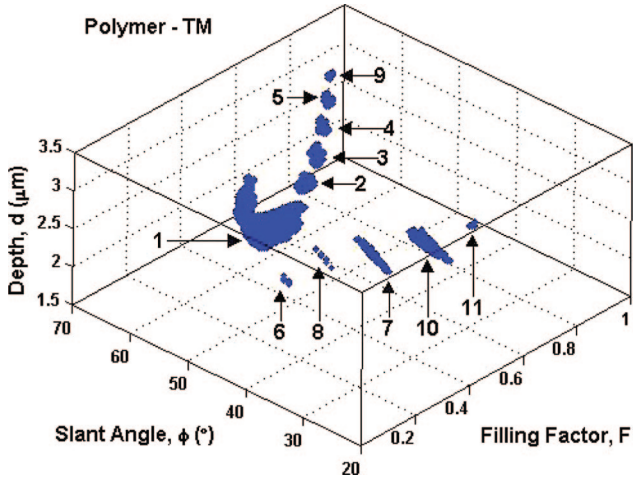

Fig. 3. (Color online) Mapped points for polymer PFSSRGs in TM operation with diffraction efficiencies greater than 96.37% in the negative-first order. There are 11 identified regions with local optima.

Table 1. Optimization of Polymer Parallel-Face Slanted Surface-Relief Gratings

Polymer PFSSRGs ($n = 1.5$, $\lambda_0 = 0.850$ μm, $\Lambda_x = 0.8014$ μm)

TE Polarization

Profile Space Region	Filling Factor F_{opt}	Slant Angle ϕ_{opt} (°)	Depth d_{opt} (μm)	$DE_{-1,opt}{}^{T}$ (%)	Estimated First Bragg Slant Angle $\phi_{Br,-1}$ (°)
P TE 1	**0.339**	**66.861**	**0.656**	**98.097**	**65.7**
P TE 2	**0.583**	**66.674**	**0.948**	**97.544**	**67.6**
P TE 3	0.260	47.000	1.645	98.333	64.5
P TE 4	0.736	66.414	1.797	98.179	68.2
P TE 5	0.262	55.602	2.243	98.531	64.5
P TE 6	0.367	60.254	2.411	98.896	66.0
P TE 7	0.272	44.774	2.597	99.188	64.7
P TE 8	0.359	67.368	2.599	97.482	65.9
P TE 9	0.464	64.031	2.697	99.215	66.9
P TE 10	0.377	40.000	2.856	96.994	66.1
P TE 11	0.436	3.961	2.905	98.962	66.7
P TE 12	0.843	66.810	2.954	97.246	68.6
P TE 13	0.531	67.957	3.040	96.898	67.3

TM Polarization

Profile Space Region	Filling Factor F_{opt}	Slant Angle ϕ_{opt} (°)	Depth d_{opt} (μm)	$DE_{-1,opt}{}^{T}$ (%)	Estimated First Bragg Slant Angle $\phi_{Br,-1}$ (°)
P TM 1	**0.444**	**59.141**	**1.894**	**98.829**	**65.1**
P TM 2	**0.726**	**63.596**	**1.900**	**98.035**	**67.6**
P TM 3	0.786	64.663	2.167	98.075	67.9
P TM 4	0.818	64.933	2.437	97.957	68.1
P TM 5	0.843	65.390	2.722	97.761	68.2
P TM 6	0.157	42.555	2.749	97.483	60.0
P TM 7	0.329	34.363	2.894	97.930	63.2
P TM 8	0.217	37.991	3.000	97.355	61.1
P TM 9	0.861	65.778	3.008	97.923	68.3
P TM 10	0.424	31.715	3.099	98.863	64.9
P TM 11	0.549	27.703	3.100	97.932	66.4

Local optima with reasonable fabrication feasibility are in bold and have had sensitivity analysis performed.

case required variation in three: the top and bottom filling factors and the slant angle. For the polymer, the sawtooth optimization produced efficiencies of 62.54% for TE and 33.94% for TM and the trapezoidal optimization produced efficiencies of 62.61% for TE and 35.68% for TM. For silicon, the sawtooth optimi-

Table 2. Optimization of Silicon Parallel-Face Slanted Surface-Relief Gratings

Silicon PFSSRGs ($n = 3.475$, $\lambda_0 = 1.550$ μm, $\Lambda_x = 0.6308$ μm)

TE Polarization

Profile Space Region	Filling Factor F_{opt}	Slant Angle ϕ_{opt} (°)	Depth d_{opt} (μm)	$DE_{-1,opt}{}^{T}$ (%)	Estimated First Bragg Slant Angle $\phi_{Br,-1}$ (°)
Si TE 1	**0.579**	**58.475**	**0.497**	**79.647**	**67.1**
Si TE 2	**0.798**	**64.982**	**1.199**	**78.125**	**68.2**
Si TE 3	0.772	23.543	2.123	70.232	68.1
Si TE 4	0.601	53.105	2.263	83.512	67.2
Si TE 5	0.904	66.303	2.318	72.290	68.6

TM Polarization

Profile Space Region	Filling Factor F_{opt}	Slant Angle ϕ_{opt} (°)	Depth d_{opt} (μm)	$DE_{-1,opt}{}^{T}$ (%)	Estimated First Bragg Slant Angle $\phi_{Br,-1}$ (°)
Si TM 1	**0.797**	**62.346**	**0.570**	**82.446**	**67.0**
Si TM 2	**0.730**	**70.715**	**1.346**	**92.068**	**66.5**
Si TM 3	0.713	35.217	1.843	99.626	66.3
Si TM 4	0.757	68.827	2.542	96.958	66.7
Si TM 5	0.700	53.556	2.884	83.066	66.1

Local optima with reasonable fabrication feasibility are in bold and have had sensitivity analysis performed.

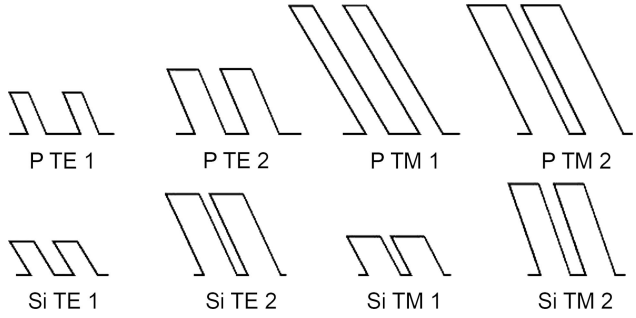

Fig. 4. Summary of optimized profiles with reasonable fabrication feasibility for both the polymer and silicon cases.

zation produced efficiencies of 47.87% for TE and 68.55% for TM, and the trapezoidal optimization produced efficiencies of 47.87% for TE and 69.09% for TM.

Wang, Jiang, and Nordin [23–25] have done important work in the area of PFSSRGs for optical coupling. Using a μGA-2D FDTD analysis, slanted grating couplers (SLGCs) for polymer and embedded slanted grating couplers (ESGCs) for silicon-on-insulator were optimized. Since these operated in the strong-coupling regime and had finite lengths, μGA-2D FDTD was used. It was found that the Bragg conditions and phase-matching conditions were based on the fundamental leaky mode, not on the output waveguide mode. Optimization was performed for uniform and nonuniform profiles, producing efficiencies of 66.8% and 80.1% in the SLGC case for profiles with uniform and nonuniform filling factors, respectively. Efficiencies of 69.8% and 75.8% were found in the ESGC case for profiles with uniform and nonuniform filling factors. Simulation times, however, were approximately two weeks for 500 μGA-2D FDTD generations. Wang, Jiang, and Nordin [25] have also developed a streamlined process for design optimization utilizing the understanding gained from previous work. This process greatly

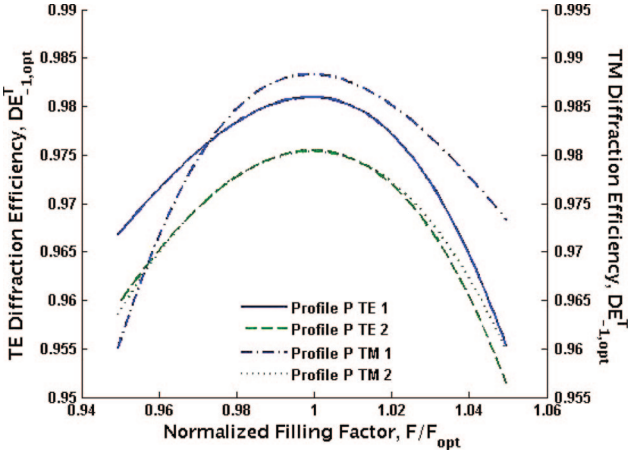

Fig. 6. (Color online) Diffraction efficiencies of polymer PFSSRGs as a function of normalized filling factor for both the TE and TM optimized profiles.

reduced simulation time and resulted in only a small deviation from results obtained via μGA-2D FDTD. It is important to note that, while this work is based on the concept that RCWA is not sufficient, the resulting discrepancy was found to be small.

3. Parallel-Face Slanted Surface-Relief Grating Optimization Technique

While much previous work has been primarily concerned with finding an optimum profile in a given simulation space, it may be the case that several optima exist, and that all of these may be of interest. To this end, a "mapping" of localized optima is desirable. The design technique put forward in this paper involves a coarse-mapping simulation, followed by localized investigation with an SA algorithm, both steps using RCWA. For PFSSRGs, the variable parameters include the depth, slant angle, and filling factor, which define a three-dimensional simulation space. The extent of the simulation space itself will depend on what is ultimately feasible for fabrication.

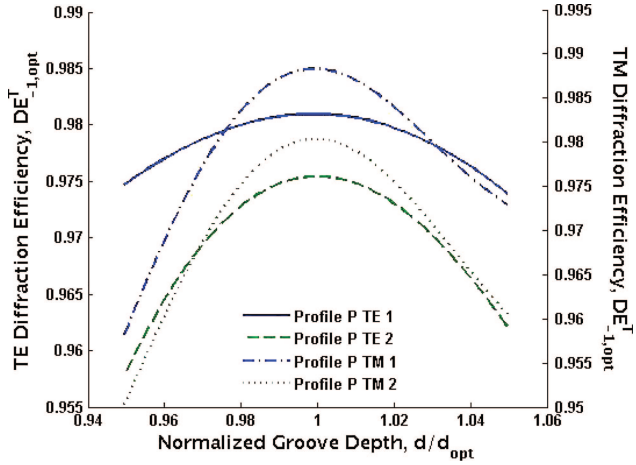

Fig. 5. (Color online) Diffraction efficiencies of polymer PFSSRGs as a function of normalized groove depth for both the TE and TM optimized profiles.

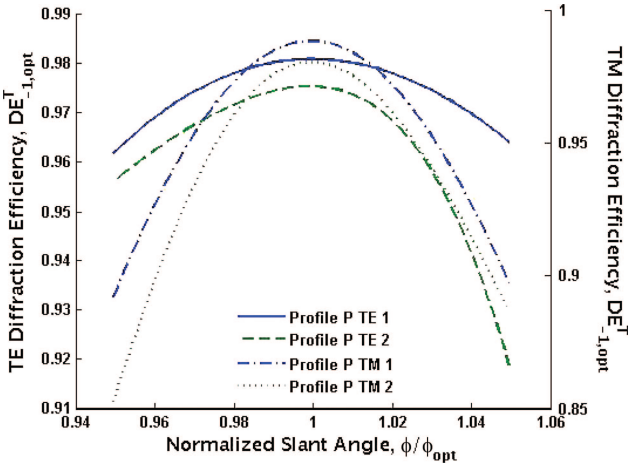

Fig. 7. (Color online) Diffraction efficiencies of polymer PFSSRGs as a function of normalized slant angle for both the TE and TM optimized profiles.

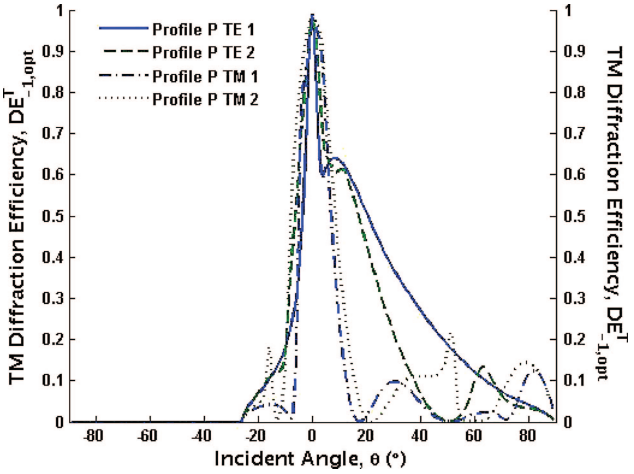

Fig. 8. (Color online) Diffraction efficiencies of polymer PFSSRGs as a function of angle of incidence for both the TE and TM optimized profiles.

The identification of localized high-efficiency regions is done manually and is appropriate for simulation spaces of three or more dimensions. The use of RCWA is not strictly applicable to gratings of finite length but is nevertheless broadly applicable to typical configurations treated here. To illustrate this process, optimization was performed for polymer and silicon cases for depths of up to 3 microns and both TE and TM polarizations at normal incidence in air with an output angle of 45° for the negative-first diffracted order. The simulated configuration is depicted in Fig. 1.

4. Simulation Results

The parameters of interest for PFSSRGs are the filling factor (equal at the top and bottom of the groove) F, slant angle ϕ, and groove depth d. To produce a mapping of high efficiencies, the bounds of the simulation space must be defined. For completeness, filling factors ranging from 0.01 to 0.99 and slant angles ranging from 1° to 89° were included. Since the limit on depth is arbitrary, an upper limit of 3 microns was used for both the silicon and polymer cases, which is approximately $2\lambda_0$ for the silicon case and $3\lambda_0$ for the polymer case. Since simulation time is at a premium and the depth limit is beyond what would be considered reasonable for fabrication, this choice of simulation space appears to be sufficient for the PFSSRG cases. All simulations were performed on 2 GHz single-processor personal computers with 1 GB of RAM.

For the polymer case, the index is $n = 1.5$, along with an incident wavelength of $\lambda_0 = 0.85$ μm. To achieve the desired output angle, a grating period of $\Lambda_x = \lambda/n \sin 45° = 0.8014$ μm was used. Figures 2 and 3 show the generated mappings for the TE and TM cases, which include 13 (TE) and 11 (TM) regions with diffraction efficiencies greater than 94.7% for TE and 96.4% for TM in the negative-first forward-diffracted order. Overall simulation time was approximately a week on a personal computer for each case using 80 sublayers, 7 diffracted orders, and 20 coefficients for the harmonic expansion of the refractive index. To reduce the simulation time for deeper gratings in the simulation space, a fixed number of subgratings were used that can portray accurately profiles of greater depth. Limiting the depth bound and fixing the number of sublayers to a fraction of the wavelength of interest is an alternative means that in some cases can reduce simulation time while maintaining accuracy.

After identifying the high-efficiency regions, an SA algorithm was used to find each local optimum. The same parameters for sublayers, diffracted orders, and number of harmonics were used, and the results for both the TE and TM cases are summarized in Table 1. The optimized gratings are ordered by increasing groove depth. Every local optimum recorded has very high efficiency, with the lowest being 96.90% in the TE case and 97.36% in the TM case. The simulation times involved varied from less than one day to as

Table 3. Summary of Optimum Profiles for the Polymer and Silicon Cases with the Highest Fabrication Feasibility

Polymer PFSSRG Optimization ($n = 1.5$, $\lambda_0 = 0.850$ μm, $\Lambda_x = 0.8014$ μm)				
	TE Optimized Profile		TM Optimized Profile	
Optimized Parameters	P TE 1	P TE 2	P TM 1	P TM 2
d_{opt} (μm)	0.656	0.948	1.894	1.900
ϕ_{opt} (°)	66.86	66.67	59.14	63.60
F_{opt}	0.339	0.583	0.444	0.726
$DE_{-1,opt}{}^T$ (%)	98.10	97.54	98.83	98.04
Silicon PFSSRG Optimization ($n = 3.475$, $\lambda_0 = 1.550$ μm, $\Lambda_x = 0.6308$ μm)				
	TE Optimized Profile		TM Optimized Profile	
Optimized Parameters	Si TE 1	Si TE 2	Si TM 1	Si TM 2
d_{opt} (μm)	0.497	1.199	0.570	1.346
ϕ_{opt} (°)	58.48	64.98	62.35	70.72
F_{opt}	0.579	0.798	0.797	0.730
$DE_{-1,opt}{}^T$ (%)	79.65	78.13	82.45	92.07

long as a week. The highest simulation times were for the least feasible cases with the shallowest slant angles and greatest depths. While the identified diffraction efficiencies for both polarizations were similar, the TM profiles were, in general, greater in depth. From the located optima, four cases were chosen that demonstrate the high efficiency with reasonable feasibility for fabrication, two cases each for TE and TM. The principal feature determining feasibility is the groove depth in relation to the slant angle. The profiles deemed most feasible were those where one ridge would least cover the next ridge and minimize any problems associated with slanted etching. The chosen cases correspond to regions 1 and 2 for TE and TM. The resulting polymer profiles are summarized in Table 3 and are shown in Fig. 4. The optimized diffraction efficiencies are 98.10%, 97.54%, 98.83%, and 98.04% for the gratings in the order listed. It should be noted that for both TE and TM, the practical case with shallower groove depth has slightly higher diffraction efficiency. The slant angle for which the first Bragg condition would be satisfied, $\phi_{\mathrm{Br},-1}$, was estimated for each grating case and is presented in Table 1. The average effective index for each polarization was calculated using the effective media formulation of Rytov for a periodic structure at long wavelengths with a given filling factor [26]. It is noteworthy that these estimated slant angles are near the optimized-profile slant angles in most cases. In fact, all of the profiles chosen for their fabrication feasibility exhibited slant angles near those that are estimated to satisfy the first Bragg condition. Sensitivity analysis was also performed for the variable parameters (d, F, and ϕ) to determine fabrication tolerances and the incident angle to determine alignment tolerance. Smoothly varying curves are shown for the parameters with 5% variation and are summarized in Figs. 5–8. These curves show modest changes in diffraction efficiency of typically a few percent, with the greatest changes due to variation of the slant angle, which showed a maximum change of slightly greater than 12%. For the incident angle, analysis was performed over the entire possible range. The loss in diffraction efficiency is modest for misalignment of less than a couple degrees, but significant for anything greater.

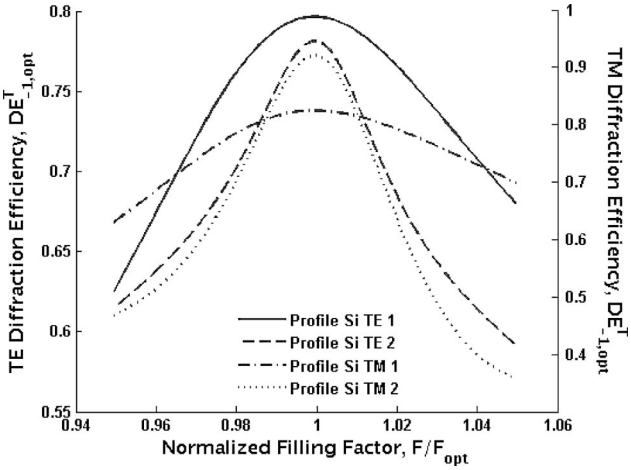

Fig. 10. Diffraction efficiencies of silicon PFSSRGs as a function of normalized filling factor for both the TE and TM optimized profiles.

For the silicon case, $n = 3.475$, $\lambda_0 = 1.55$ μm, and $\Lambda_x = 0.6308$ μm. The generated mappings for the TE and TM cases resulted in five high-efficiency regions for each case. After performing SA, the optimized results are summarized in Table 2 where they are again ordered by increasing groove depth. The simulation parameters were identical to those for the polymer case. As is consistent with previous work on silicon SRGs [21,22], these gratings are more appropriate for TM polarization as they demonstrate much higher efficiencies than for TE polarization. Efficiencies for TE range from 70.23% to 83.51%, while TM efficiencies range from 82.45% to 99.63%. For each case, two feasibly fabricated optima are identified as shown in Table 2. These optima correspond to regions

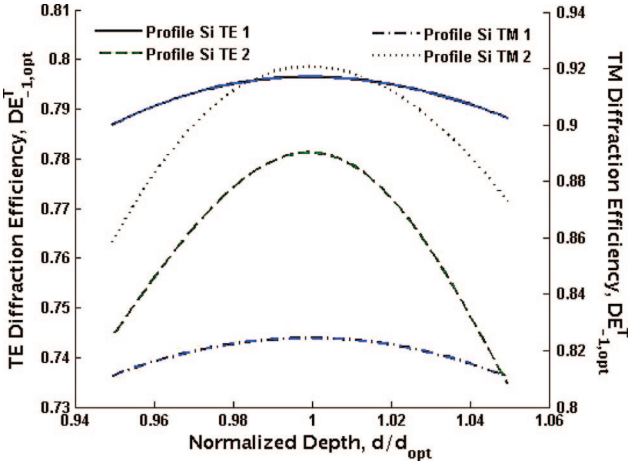

Fig. 9. (Color online) Diffraction efficiencies of silicon PFSSRGs as a function of normalized groove depth for both the TE and TM optimized profiles.

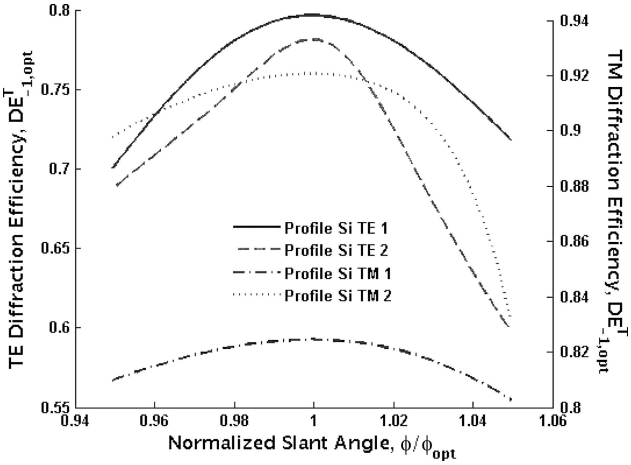

Fig. 11. Diffraction efficiencies of silicon PFSSRGs as a function of normalized slant angle for both the TE and TM optimized profiles.

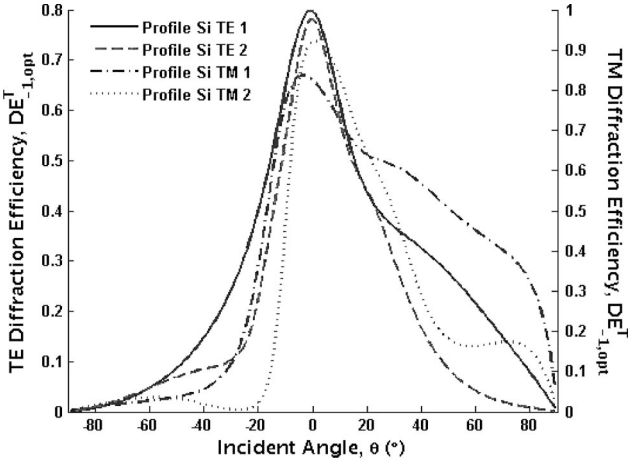

Fig. 12. Diffraction efficiencies of silicon PFSSRGs as a function of angle of incidence for both the TE and TM optimized profiles.

1 and 2 for TE and for TM. Summarized results for these profiles are provided in Table 2, and the profiles are shown in Fig. 4. The optimized efficiencies are 79.65%, 78.12%, 82.44%, and 92.07% for the gratings in the order listed. While for TE the shallower practical case has higher diffraction efficiency similar to the polymer case, for TM it is the opposite, and the difference is a significant 10%. Slant angles estimated to satisfy the first Bragg condition for given filling factor are also presented in Table 2. Again, most of the optimized profiles exhibit slant angles near those that are estimated to satisfy the first Bragg condition. These first Bragg slant angles were determined in the same manner as those for the polymer case. As with the polymer case, all of the profiles chosen for their feasible fabrication have slant angles near those that are estimated to satisfy the first Bragg condition. Sensitivity analysis was performed in a fashion similar to that for the polymer case and is presented in Figs. 9–12. The silicon gratings are more tolerant to misalignment than the polymer gratings but exhibit higher sensitivity to changes in depth, filling factor, and slant angle. The only extreme sensitivity is to filling factor for the TM profiles, with the diffraction efficiency dropping almost 60% with 5% variation. Simulation times were similar to those for the polymer case.

5. Summary and Conclusions

We have determined optimum PFSSRGs utilizing RCWA and combining an exhaustive approach with a SA algorithm. The method was demonstrated for polymer and silicon cases over a large simulation space, several optimized profiles were found, and some key profiles with strong fabrication feasibility were further analyzed and showed modest sensitivities to fabrication and alignment variations. Four optimized profiles were chosen for the polymer and silicon cases that can feasibly be fabricated; there were two cases each for TE and TM optimizations. All of the optimized profiles chosen for their fabrication feasibility exhibited slant angles that were near those that are estimated to satisfy the first Bragg condition. For the polymer case, all of the cases have diffraction efficiencies greater than 97%, but for TM polarization, the profiles require greater depth. In the silicon case, the diffraction efficiencies of the TM profiles are significantly greater than the TE profiles; for TM, the efficiencies are 82% (Si TM 1) and 92% (Si TM 2), while for TE, the efficiencies are 79% (Si TE 1) and 78% (Si TE 2). For the practical cases chosen for TE and TM, the profiles with smaller groove depths have slightly higher diffraction efficiency, with the exception of the silicon TM case in which the deeper profile has significantly greater diffraction efficiency. The polymer profiles show modest changes in diffraction efficiency over 5% of grating parameters, and the greatest change comes from variation in the slant angle. These profiles are reasonable sensitive to the alignment however. The silicon profiles are more tolerant to alignment but less tolerant to fabrication error, and there is a very strong sensitivity to the filling factor for the TM case.

The key advantage of this approach is the location of several localized optima within a simulation space. For given design constraints, several optima may exist that may have various advantages and disadvantages, and it is of interest not to overlook any potential profiles that may provide other benefits. For example, it may be desired to have high diffraction efficiency in multiple orders. With the availability of fabrication techniques such as ENABLE, high-efficiency PFSSRGs have many potential applications, and a broadly applicable and flexible design process is necessary.

References

1. S. Ura, T. Suhara, H. Nishihara, and J. Koyama, "An integrated-optic disk pickup device," J. Lightwave Technol. **4,** 913–918 (1986).
2. J. M. Miller, N. de Meaucoudrey, P. Chavel, J. Turunen, and E. Cambril, "Design and fabrication of binary slanted surface-relief gratings for a planar optical interconnection," Appl. Opt. **36,** 5717–5727 (1997).
3. R. T. Chen, L. Lin, C. Choi, Y. J. Liu, B. Bihari, L. Wu, S. Tang, R. Wickman, B. Picor, M. K. Hibbs-Brenner, S. Bristow, and Y. S. Liu, "Fully embedded board-level guided-wave optoelectronics interconnects," Proc. IEEE **88,** 780–793 (2000).
4. A. V. Tishchenko, N. M. Lyndin, S. M. Loktev, V. A. Sychugov, and B. A. Usievich, "Unidirectional waveguide grating coupling by means of parallelogramic grooves," Proc. SPIE **3099,** 269–277 (1997).
5. V. A. Sychugov, A. V. Tishchenko, B. A. Usievich, and O. Parriaux, "Optimization and control of grating coupling to or from a silicon-based optical waveguide," Opt. Eng. **35,** 3092–3100 (1996).
6. D. Taillaert, W. Bogaerts, P. Bienstman, T. F. Krauss, P. Van Daele, I. Moerman, S. Verstuyft, K. De Mesel, and R. Baets, "An out-of-plane grating coupler for efficient butt-coupling between compact planar waveguides and single-mode fibers," IEEE Quantum Electron. **38,** 949–955 (2002).
7. B. D. Clymer, "Surface-relief grating structures for efficient high-bandwidth integrated photodetectors for optical interconnections in silicon VLSI," Appl. Opt. **28,** 5374–5382 (1989).
8. E. Dupont, "Optimization of lamellar gratings for quantum-well infrared photodetectors," Appl. Phys. **88,** 2687–2692 (2000).

9. A. Hamori and N. Nagy, "Sub-micrometer period refractive index grating coupler for single mode optical waveguide sensors," Proc. IEEE Sensors **3,** 1333–1336 (2004).
10. N. Kinrot and M. Nathan, "Investigation of a periodically segmented waveguide Fabry–Pérot interferometer for use as a chemical/biosensor," J. Lightwave Technol. **24,** 2139–2145 (2006).
11. D. Taillaert, R. Baets, P. Dumon, W. Bogaerts, D. van Thourhout, B. Luyssaert, V. Wiaux, S. Beckx, and J. Wouters, "Silicon-on-insulator platform for integrated wavelength-selective components," in *Fourth IEEE/LEOS Workshop on Fibers and Optical Passive Components* (IEEE, 2005), pp. 115–120.
12. D. L. Brundrett, T. K. Gaylord, and E. N. Glytsis, "Polarizing mirror/absorber for visible wavelengths based on a silicon subwavelength grating: design and fabrication," Appl. Opt. **37,** 2534–2541 (1998).
13. Y. Li, D. Chen, and C. Yang, "Sub-microns period grating couplers fabricated by silicon mold," Opt. Laser Technol. **33,** 623–626 (2001).
14. M. Okano, H. Kikuta, Y. Hirai, K. Yamamoto, and T. Yotsuya, "Optimization of diffraction grating profiles in fabrication by electron-beam lithography," Appl. Opt. **43,** 5137–5142 (2004).
15. H. Nakano, T. Tanino, and Y. Shirota, "Surface relief grating formation on a single crystal of 4-(dimethylamino)azobenzene," Appl. Phys. Lett. **87,** 061910 (2005).
16. E. A. Akhadov, A. H. Mueller, and M. A. Hoffbauer, "Energetic neutral atom beam lithography/epitaxy for nanoscale device fabrication," Mater. Res. Soc. Symp. Proc. **872,** 503–506 (2005).
17. E. A. Akhadov, D. E. Read, A. H. Mueller, J. Murray, and M. A. Hoffbauer, "Innovative approach to nanoscale device fabrication and low-temperature nitride film growth," J. Vac. Sci. Technol. B **23,** 3116–3119 (2005).
18. A. H. Mueller, E. A. Akhadov, and M. A. Hoffbauer, "Low-temperature growth of crystalline GaN films using energetic neutral atomic-beam lithography/epitaxy," Appl. Phys. Lett. **84,** 041907 (2006).
19. T. K. Gaylord and M. G. Moharam, "Analysis and applications of optical diffraction by gratings," Proc. IEEE **73,** 894–937 (1985).
20. M. G. Moharam and T. K. Gaylord, "Diffraction analysis of dielectric surface-relief gratings," J. Opt. Soc. Am. **72,** 1385–1392 (1982).
21. S. D. Wu, T. K. Gaylord, J. S. Maikisch, and E. N. Glytsis, "Optimization of anisotropically etched silicon surface-relief gratings for substrate-mode optical interconnects," Appl. Opt. **45,** 15–21 (2006).
22. S. D. Wu, T. K. Gaylord, and E. N. Glytsis, "Optimization of sawtooth surface-relief gratings: effects of substrate refractive index and polarization," Appl. Opt. **45,** 3420–3424 (2006).
23. B. Wang, J. Jiang, and G. P. Nordin, "Compact slanted grating couplers," Opt. Express **12,** 3313–3326 (2004).
24. B. Wang, J. Jiang, and G. P. Nordin, "Embedded slanted grating for vertical coupling between fibers and silicon-on-insulator planar waveguides," IEEE Photon. Technol. Lett. **17,** 1884–1886 (2005).
25. B. Wang, J. Jiang, and G. P. Nordin, "Systematic design process for slanted grating couplers," Appl. Opt. **45,** 6223–6226 (2006).
26. S. M. Rytov, "Electromagnetic properties of a finely stratified medium," Sov. Phys. JETP **2,** 466–475 (1956).